Energy & Buildings 300 (2023) 113633

Contents lists available at ScienceDirect

Energy & Buildings

journal homepage: www.elsevier.com/locate/enbuild

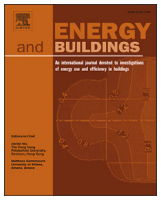

Optimal sizing and operation of seasonal ice thermal storage systems

Jacopo Vivian [a,*], Philipp Heer [b], Massimo Fiorentini [c]

[a] University of Padova, Department of Industrial Engineering, via Venezia 1, 35131 Padova, Italy
[b] Empa - Swiss Federal Laboratories for Materials Science and Technology, Urban Energy Systems Laboratory, Ueberlandstrasse 129, 8600 Dübendorf, Switzerland
[c] Aarhus University, Department of Civil and Architectural Engineering, Inge Lehmanns Gade 10, 8000 Aarhus C, Denmark

ARTICLE INFO

Keywords:
Seasonal thermal energy storage
MIQCP
Design optimization
Multi-energy systems
District heating and cooling
Latent heat exchange

ABSTRACT

Ice storage systems can be used as an efficient cooling source during summer, as well as a heat source for heat pumps during winter. The non-linear behavior of the heat exchange process in storage makes formulations for optimizing the design and operation of these technologies complex. In this work, we propose a quadratically-constrained mixed-integer programming formulation, that can capture the latent and sensible behavior of the storage and its impact on the delivery of heating and cooling. A building demonstrator integrating an ice storage device was used as a case study. Monitoring data were used to validate the simplified ice storage model employed in the optimization. Results showed that the most common optimal storage cycle requires freezing the water during late winter and when the air temperature falls below 0 °C. Increasing the storage volume increases both storage efficiency and the amount of free cooling available during summer. For these reasons, economies of scale can make larger systems more competitive than smaller ones. Storage size and thermal insulation level affect the duration of the charging and discharging phases. Thermal insulation improves seasonal efficiency and free cooling significantly. A higher CO_2 emissions price does not yield significant benefits in terms of emissions reductions. High investment costs and the seasonal variation in CO_2 intensity of electricity reduce the economic and environmental competitiveness of long-term ice storage systems, respectively.

1. Introduction

Thermal Energy Storage (TES) denotes a set of technologies that allow heat energy to be captured and retained in a medium for later use. This is particularly important due to the temporal mismatch between renewable generation and the demand for space heating and cooling. TESs are commonly classified into three main types depending on the mechanism that occurs when heat is supplied and released from the storage [1]. In sensible heat storage systems, the medium changes temperature; in latent heat storage systems, the medium changes phase (e.g. from solid to liquid and vice versa); and in thermochemical heat storage systems, the concentration of a solvent in a solution changes.

1.1. Seasonal thermal energy storage systems

Seasonal thermal storage systems are conceived to reduce the temporal gap between periods with high renewable energy available and periods with high energy demand. In heating-dominated climates, this means storing renewably-generated heat (typically from solar panels) or waste heat from cooling operations during summer to be used later in winter. Storing the heat for such a long term requires large systems, normally connected to high investment costs, thus making these large systems economically attractive when economies of scale can be leveraged [2]. The most mature technologies are based on sensible heat storage, such as tanks, pits, boreholes, and aquifers [2]. Latent heat storage systems based on Phase Change Materials (PCM) such as salt hydrates or paraffin waxes, as well as thermochemical storage systems, show a high potential due to their high energy density, but also a lower technological maturity and higher risks due to the corrosion, flammability, and toxicity of these substances [2].

1.1.1. Ice storage systems

Ice storage systems are not subject to these problems since they employ water as a storage medium, which is an available and environmentally friendly medium. The expression “ice storage” commonly defines thermal storage employing the enthalpy difference of water during its phase change from liquid to solid [3]. The high latent heat of fusion of water results in a higher energy density for this type of storage compared to water-based sensible storage, leading to smaller volumes. Since the melting temperature of water is 0 °C, ice storage

* Corresponding author.
E-mail address: jacopo.vivian@unipd.it (J. Vivian).

https://doi.org/10.1016/j.enbuild.2023.113633
Received 13 June 2023; Received in revised form 19 September 2023; Accepted 9 October 2023
Available online 16 October 2023

Nomenclature

ϵ	water volume in the storage (%)
η	efficiency (%)
λ	specific price (CHF/unit)
ρ	density (kg/m^3)
b	branch (–)
c_p	specific heat capacity (kJ/kg K)
D	diameter (m)
d	downstream node/branch (–)
E_{CO_2}	CO_2 emissions (kg/y)
H	time steps of optimization horizon (–)
h	height (m)
h_f	latent heat of fusion (kJ/kg)
i	specific investment cost (CHF/unit)
M	constant (–)
N	subset of nodes/branches (–)
n	node (–)
P	power (kW)
Q	heat (kJ)
S	surface area (m^2)
s	sensible heat exchange (0/1)
T	temperature (°C)
t	time step (–)
T_f	melting temperature (°C)
U	heat transfer coefficient (W/m^2 K)
u	upstream node/branch (–)
V	volume (m^3)
y	year (–)

Subscripts and superscripts

av	available
bp	bypass
cd	condenser
ch	charge
$chill$	chiller
$cool$	cooling
$disch$	discharge
el	electrical
ev	evaporator
exp	exported
gnd	ground
hp	heat pump
hs	heat source for heat pumps / heat sink of chillers
hx	heat exchanger
i	ice
imp	imported
l	lateral
lat	latent heat exchange
max	maximum
$sens$	sensible heat exchange
st	storage
su	supply
w	water

Acronyms

COP	Coefficient Of Performance
MIQCP	Mixed Integer Quadratically-Constrained Programming
LCOE	Levelized Cost Of Energy
FCR	Free Cooling Ratio
SCOP	Seasonal Coefficient Of Performance
SEER	Seasonal Energy Efficieny Ratio
ASHP	Air-Source Heat Pump
WWHP	Water-to-Water Heat Pump
TES	Thermal Energy Storage
PCM	Phase Change Materials
CAPEX	Capital expenditure
OPEX	Operational expenditure

systems are used as a heat source during the heating season, to provide free cooling during summer. Ice storages are normally employed for demand peak shaving rather than seasonal load shifting, and are therefore limited in size with a clear operation objective [4,5]. This holds particularly true in applications, such as refrigeration in supermarkets, where high cooling demands and fluctuation in electricity prices make these systems economically attractive [6]. They are also employed as longer-term thermal energy storage devices, as presented in [7], where the ice storage balances the heat rejected from summer cooling operations and the heat extracted by a heat pump in winter for space heating.

Research conducted on ice storage systems, generally employed high-detail models to estimate the performance of such systems. For example, Carbonell et al. [3] developed an ice storage model based on a transient one-dimensional energy equation derived along the height of the storage. The model was coupled to a ground model, which was solved with a transient heat conduction equation using the ice storage as a heat source. The validation with experimental measurements of 75 m^3 ice storage model buried in the ground showed good agreement in terms of heat extracted from the storage and ground temperatures above and below the storage. Measured ground temperatures on the sides of the storage were instead over-estimated by the model. Allan et al. [8] proposed a simpler model based on three thermal capacitances using undisturbed ground temperature as a boundary condition. They used the model to calibrate the heat loss coefficients of two ice storage systems buried in the ground. One of them (the same shown here in Section 3) showed very high heat loss in the bottom part, probably due to the effect of a groundwater flow.

One important consideration in designing an ice thermal storage system is the size of the storage tank. The size of the tank must be sufficient to store enough ice to meet a sufficient portion of the cooling demand during summer, but it should not be so large that it becomes unnecessarily costly to be constructed and integrated. Optimizing the size of the ice tank, together with its expected operation and estimation of reduction in operating costs, is therefore crucial to ensure that such an investment can be fully exploited in the lifetime of the system [9]. The optimal tank size depends on factors such as the cooling load of the building, the duration of the peak demand period, the construction and thermal losses of the tank and the rate at which the ice can be formed and melted.

Another important consideration is the design of the heat extraction system, effectively forming the ice, to produce the required amount of ice in the available storage volume. It is also important to ensure that the system using ice as a source operates efficiently, especially at times when other heat sources are less convenient (e.g., when the ambient air temperature is sub-zero).

1.1.2. Optimization of seasonal thermal energy storage systems

Optimizing seasonal storage design and operation has been the subject of recent studies. Gabrielli et al. [10] proposed a mixed integer linear program methodology to optimize the design of a seasonal storage with hourly resolution using typical days. Fiorentini et al. [11], with a similar objective, formulated a quadratically-constrained problem that can also model the temperature dynamics of the borehole thermal energy storage, considering the influence of the seasonal storage size and temperature on the capacity, losses, heat transfer rate, and efficiency

of connected heat pumps or chillers. The study showed that the cost of CO_2 and the ratio between cooling and heating demand affect not only the optimal size of the seasonal storage and the amount of solar collectors, but also the optimal temperature profile, i.e., how the operation should be changed in order to minimize costs and CO_2 emissions. In a similar study, the authors introduced a further degree of freedom by allowing heat to flow through a by-pass instead of being extracted by a heat pump during the winter season [12]. It was found that the by-pass can only be used for a short time at the beginning of the heating season, when the average temperature of the boreholes is higher or equal to the supply temperature of the thermal grid.

Because of phase transitions, ice storage models such as those mentioned in Section 1.1.1 are not linear. Therefore, when they are implemented as constraints of optimization problems, ice storage models are either simplified to state-of-charge models (e.g., [13], [14]) or rely on stochastic optimization models such as Genetic Algorithms, Particle Swarm Optimization (e.g. [15]) etc. In the former case, models fail in reproducing the temperature of the storage when the ice in the storage is completely melted or completely frozen, i.e., when sensible heat is exchanged in liquid or solid phase, respectively. In the latter case, the search space must be limited to define the optimal operation within an acceptable computation time. Therefore, a global optimum can only be achieved on a subset of solutions, such as predefined control strategies. An alternative to these approaches would be to simplify the physical models without losing their main characteristics (i.e., latent heat of fusion, melting temperature, latent vs sensible heat exchange based on average storage temperature). A similar approach was followed for the optimal control of a building with PCM thermal storage [16].

Designing an ice storage would require detailed modeling of the phase change occurring in the storage, which in turn depends on many factors such as geometry and layout of the internal coils, diameter and height of the storage tank, etc. (see for instance [17,18]) and goes beyond the objectives of this paper. However, the optimal size of the storage (nominal capacity) can be determined based on the application, i.e., on the boundary conditions (heating and cooling loads, air and ground temperature, etc.) of the considered case study.

As a summary, the literature shows that there is a need for an optimization framework that can tackle the combined optimization of both design and control of an ice storage which is meant to be employed to shift loads at a seasonal scale.

1.2. Research gap and contribution

While the optimization of the design and operation of energy systems with seasonal thermal energy storage has been the focus of several recent research efforts, there is a clear gap in the literature on the optimization of systems employing ice storage systems, particularly for seasonal energy storage purposes.

Furthermore, optimal design methods require suitable optimization-oriented modeling techniques for this type of storage device, which are also missing in the literature.

This study proposes an optimization approach, based on a quadratically-constrained mixed integer programming formulation, that can assist the decision-making on the sizing and operation of a heating and cooling system integrating an ice storage device, together with an appropriate optimization-oriented model that describes the most important thermal behavior aspects of ice storage systems.

2. Methods

2.1. Optimization problem

The energy hub problem considered in this study is defined through a set of interconnected nodes and branches, describing the energy system. Each node is associated with one of the following node classes: junction, storage, converter, exchange, load boundary or temperature boundary. Each branch is associated with an energy carrier (e.g., heat, electricity etc). A graphical representation of the generic energy system with an ice storage studied in this paper is presented in Fig. 1.

2.1.1. Ice storage constraints

To represent the state in which the ice storage is, either in a melting phase or liquid, a time-varying binary variable $s(t)$ is employed to model the two different heat balances occurring in the two phases: if the average temperature is higher or equal to the melting temperature T_f, the heat ice storage is operating in its sensible range and $s(t) = 1$. Vice versa, when the temperature is lower or equal to the melting temperature, the storage is operating in its latent range and $s(t) = 0$. This conditional statement is formulated using a big-M, with the constraints in Eq. (1):

$$\begin{cases} T(t, n_{st}) \geq T_f - M(1 - s(t)), \\ T(t, n_{st}) \leq T_f + M s(t) \end{cases} \tag{1}$$

where n_{st} is the node of the ice storage in the energy hub. The energy balance of the storage depends on the value of the mentioned binary variable. When the storage is operating in its latent range, the heat exchange does not affect the storage temperature T the heat transferred to/from the storage determines the ratio of water in the storage, $\epsilon(t)$, which can vary between 0 (all ice) and 1 (all water). This process is modeled in Eq. (2).

$$s(t) = 0 \implies \begin{cases} T(t, n_{st}) = T_f, \\ \rho_i V_{st} h_f \frac{\epsilon(t) - \epsilon(t - \Delta t)}{\Delta t} = \sum_{u \in N_u} P(t, u) - \sum_{d \in N_d} P(t, d) - \\ U A_{st} (T(t, n_{st}) - T_{gnd}) \end{cases} \tag{2}$$

Where N_u and N_d are the subsets of upstream and downstream branches of node n, respectively. As we assumed that once the water in the storage is completely frozen, ice cannot be cooled further (i.e., below 0 °C), $\epsilon(t) = 0$ represents the maximum state of charge of the ice storage, i.e., the state when no heat can be further extracted from the storage. When $\epsilon(t) = 1$, only water is present in the storage, and if heat is supplied to it, the water temperature increases. This process is presented in Eq. (3).

$$s(t) = 1 \implies \begin{cases} \epsilon(t) = 1, \\ \rho_w V_{st} c_{p,w} \frac{T(t, n_{st}) - T(t - \Delta t, n_{st})}{\Delta t} = \sum_{u \in N_u} P(t, u) - \sum_{d \in N_d} P(t, d) - \\ U A_{st} (T(t, n_{st}) - T_{gnd}) \end{cases} \tag{3}$$

To represent the physical limits in heat transfer from the storage, an upper limit was imposed on the maximum heat flow rate that could be exchanged by the heat transfer fluid in the storage. Although in ice-on-coil systems it is common that the thermal resistance increases with the ice build-up on the coils [19,8], thus reducing the heat transfer in the latent phase, data from the monitored system at Empa [8] do not show an appreciable correlation between the heat flow rate during ice formation and the amount of ice in the storage. This was probably due to a combination of two factors: (1) the ice storage was generally operating with low amounts of ice and (2) the bottleneck in heat exchange was the upstream evaporator of the glycol-to-water heat pump, instead of the storage. Therefore, a constant value was used to determine the maximum heat transfer coefficient of the storage, $U A_{hx}$. This resulted in the definition of two constraints, one for charging and one for discharging, when the ice storage is in the latent phase, as shown in Equations (4) and (5).

$$\sum_{d \in N_d} P(t, d) \leq U_{hx} A_{hx} \Delta T_{ch} \tag{4}$$

$$\sum_{u \in N_u} P(t, u) \leq U_{hx} A_{hx} \Delta T_{disch}. \tag{5}$$

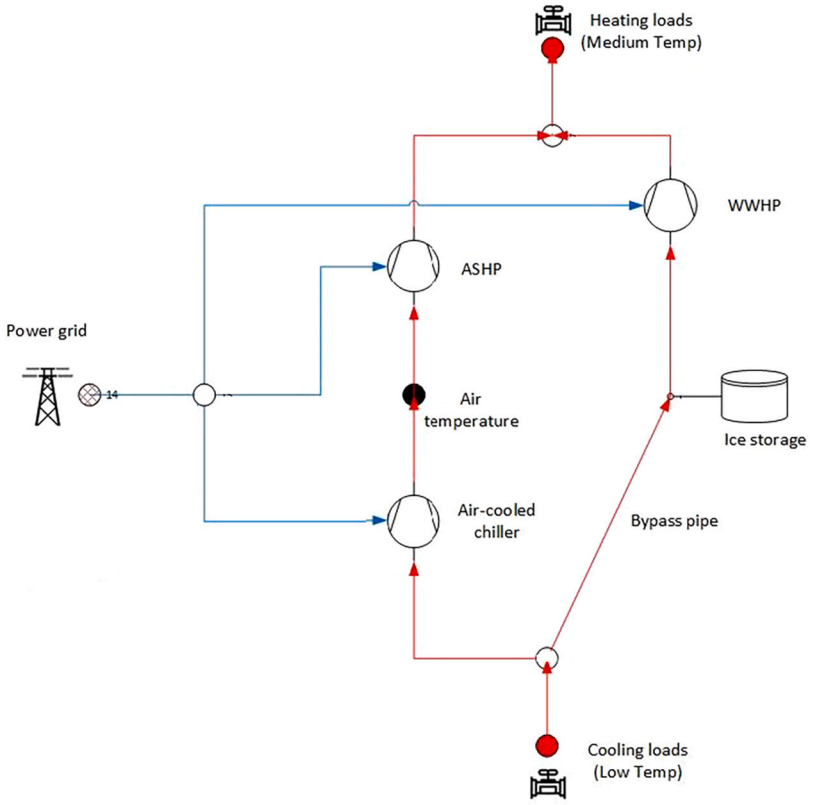

Fig. 1. A schematic of the energy hub including the ice storage.

Again, N_u and N_d are the subsets of upstream and downstream branches of node n_{st}, respectively. Some additional constraints are considered to avoid overestimating the heat rejected in the ice storage through the bypass pipe. Indeed, the latter depends on the "available cooling energy" in the storage, which consists of two parts: latent ($Q_{lat,av}$) and sensible ($Q_{sens,av}$) energy. They are defined in Equations (6) and (7), respectively. The latent residual energy is a function of the amount of ice in the storage (1 - $\epsilon(t)$), while the sensible residual energy is a function of the temperature of the storage $T(t)$.

$$Q_{lat,av}(t) = \rho_i V_{st} h_f (1 - \epsilon(t)) \tag{6}$$

$$Q_{sens,av}(t) = max\{\rho_w V_{st} c_{p,w} (T_{cool,su} - T(t, n_{st})), 0\} \tag{7}$$

Thus, the heat that can be rejected in the storage at each time step t is constrained by Eq. (8):

$$\begin{cases} P(t, u_{bp}) \geq 0 \\ P(t, u_{bp}) \leq \frac{1}{\Delta t}(Q_{lat,av}(t) + Q_{sens,av}(t)) \end{cases} \tag{8}$$

where u_{bp} is a "by-pass" upstream branch of the storage, i.e., a branch that is not connected to a converter such as a heat pump or chiller.

Lastly, two constraints are employed to ensure a cyclical behavior of the storage, forcing that both the storage temperature and ice level are equal at the beginning and at the end of the year, as in Eq. (9):

$$\begin{cases} T(1, n_{st}) = T(H, n_{st}) \\ \epsilon(1) = \epsilon(H) \end{cases} \tag{9}$$

2.1.2. Heat pump and chiller constraints

In the optimization, all heat pumps (chillers) were modeled assuming that the inverse of the Coefficient Of Performance (COP), i.e., the ratio between the absorbed electrical power and the heat exchanged at the condenser, is a linear function of the average evaporating (condensing) temperature. The latter is calculated using the heat source (heat sink) temperature, and its corresponding mean temperature difference. Therefore, the following holds true for heat pumps:

$$COP^{-1} = \frac{P_{el,hp}}{P_{cd}} = c_0 + c_1(T_{hs} - \Delta T_{ev}) \tag{10}$$

where T_{hs} is the heat source temperature, ΔT_{ev} is the mean temperature difference in the evaporator. For chillers, a similar equation was considered, where T_{hs} is the heat sink temperature and ΔT_{cd} is the mean temperature difference in the condenser:

$$COP^{-1} = \frac{P_{el,chill}}{P_{ev,chill}} = c_0 + c_1(T_{hs} + \Delta T_{cd}). \tag{11}$$

For both heat pumps and chillers, the coefficients c_0 and c_1 can be obtained using a simple linear regression as a function of the heat source and heat sink temperatures, respectively. In such a case, ΔT_{ev} and ΔT_{cd} are equal to 0 and the constraints can be simplified as shown in (12):

Equations (10) and (11) can be generalized as follows:

$$P(t, u_{el}) = P(t, d)(c_0 + c_1 T(t, n)) \tag{12}$$

The latter hold true for time step t and assuming the heat pump (chiller) corresponds to the n^{th} node of the energy hub, with u_{el} being the upstream branch with electricity as an energy carrier, and d being the downstream branch.

2.1.3. Grid exchange constraints

Some nodes in the energy hub serve as gateways where energy can be exchanged with the grid. The latter can be e.g., the electricity network if the adjacent branch has electricity as energy carrier, a thermal network if it has heat as energy carrier, etc. Assuming n is an exchange node of the energy hub, the imported and exported energy are defined using the following Equations:

$$P_{imp}(t, n) = max\{P(t, d), 0\} \tag{13}$$

$$P_{exp}(t,n) = min\{P(t,d),0\} \quad (14)$$

The above notation holds true if and only if the power flow in the downstream branch flows towards the energy hub (i.e., not towards the node n but in the opposite direction). This way, the imported and exported energy takes positive and negative values, respectively.

2.2. Optimal design procedure

The energy balance of the ice storage is expressed as a function of the time-variant binary variable $s(t)$, which turns into multiplying $s(t)$ by all the other decision variables, i.e., the power rates $P(t,b)$ for all branches b and times t and the states $T(t,n)$ and $\epsilon(t)$ for all times t. This makes Equations (2) and (3) bilinear constraints. As such, the volume of the storage can not be a decision variable and is fixed to a predefined constant value V_{st}. Therefore, a set of ice storage volumes have been defined depending on the cooling demand of the case study building.

2.2.1. Size constraints

The proposed optimization framework is meant to find the optimal design and operation of the given energy system, represented as an energy hub. Therefore, the size of all the components has been defined as:

$$V(n) \geq P(t,b) \forall t \in H \quad (15)$$

where V is the size (not necessarily a volume) of the component corresponding to node n, and b is the upstream/downstream branch connected to it. In the energy hub considered here, there are only two components (nodes) that contribute to the investment cost: the ice storage and the air-cooled chiller. As far as the ice storage is concerned, the volume was considered in a discrete manner - i.e., an optimization run was performed for each size, determining the optimal size. Therefore, in each individual optimization, the volume was considered constant as mentioned in Section 2.2.

2.2.2. Objective function

The objective function of the optimization problem is:

$$f = \sum_{n=1}^{nn} V(n) i(n) + \sum_{n=1}^{nn_x} \sum_{t=0}^{H} \lambda_{imp} P_{imp}(t,n) + \lambda_{exp} P_{exp}(t,n) + \lambda_c c(t) P_{imp}(t,n) \quad (16)$$

The optimization problem is formulated as a design optimization, because it minimizes both the investment costs (first summation in Eq. (16)) and the operating costs (second summation). However, the ice storage volume is not a decision variable, as explained above. Therefore, in the specific problem analyzed in this paper, the sum of the investment costs is reduced to a single term -the cooling capacity of the air chiller- and the investment cost for the ice storage was added a posteriori. The optimization problem is repeated for different volumes, which are predefined according to the cooling demand of the building. The results of each optimization are then compared to find the optimal volume of the ice storage including both investment and operating costs. Since the only exchange node of the energy hub is the connection to the electricity grid, λ_{imp} and λ_{exp} are the prices associated with imported and exported electricity, respectively. The price λ_c is the cost of emitted CO_2 and $c(t)$ is the time-varying CO_2 intensity of electricity.

Thus, the cost function couples together the CO_2 emissions and costs (investment and operational) through the weighting factors λ_c and λ_{imp}. The thermal performance is implicitly considered, e.g. through the dependence of the COP to the storage temperature, affecting both costs and emissions.

The optimization problem can be formulated as the minimum of f subject to constraints (1)-(15). The horizon H is one year, with a time-step of 8 hours. Such a time step allows the partial capture of intra-day effects.

The optimization used Gurobi as a solver, because the latter is able to find a global optimum to Mixed Integer Quadratically-Constrained Programming (MIQCP) problems [20]. The mathematical models were formulated using Python's interface Gurobipy. The optimization runs were performed on an Intel Quad Core i7-10510U with 32 GB DDR4 RAM.

2.2.3. Seasonal performance indicators

A set of performance indicators was used to assess the performance of the ice storage and of the other components of the considered energy system. The most important one is the Levelized Cost Of Energy (LCOE), which is directly proportional to the objective function f reported in Equation (16), which is only divided by the sum of the heating and cooling loads. LCOE refers to the energy supplied to the building for both space heating and space cooling. The heat for domestic hot water production and the electricity for other uses have not been considered here to facilitate the interpretation of the results.

Other two indicators have been used to assess the seasonal performance of the ice storage. Its seasonal efficiency η_{st} is defined as the ratio between the heat rejected into the storage via the bypass pipe on the upstream branch (u_{bp}) and the heat extracted by the water-to-water heat pump, i.e., the heat flowing through the downstream pipe (d). This definition has the useful effect of the ice storage (providing "free cooling" to the building) at the numerator and the corresponding energy cost at the denominator. In fact, extracting heat from the storage has a cost due to the electricity needed to drive the compressors of the Water-to-Water Heat Pump (WWHP). Heat gains from the surrounding ground contribute to an increase of heat that must be extracted from the storage in order to keep it at the required temperature.

$$\eta_{st} = \frac{\sum_{t \in H} P(t, u_{bp})}{\sum_{t \in H} P(t,d)} \quad (17)$$

The ice storage in none of the considered sizes is able to cover the entire cooling demand. Therefore a similar indicator (Free Cooling Ratio (FCR)) has been introduced to compare the "free-cooling" supplied to the overall cooling demand of the building:

$$FCR = \frac{\sum_{t \in H} P(t, u_{bp})}{\sum_{t \in H} P_{cool,dem}(t)} \quad (18)$$

3. Case study

3.1. System description

Fig. 2 shows the building demonstrator NEST which was used as a case study. NEST is a four-storey modular building consisting of a concrete "backbone" and a variable number of units including offices, apartments, meeting rooms, work stations, a fitness room etc. Monitored data of outdoor air temperature, heating and cooling demand for the year 2021 have been used as boundary conditions for the optimization described above, and are shown in Fig. 3.

As shown in this Figure, the net demand between heating and cooling was considered, although there are some days in the year (during spring and late summer) when the considered building has both heating and cooling demand. The net demand represents the useful energy to charge and discharge the storage, since simultaneous charging and discharging of the storage was not considered. Such assumption was found to improve the optimization speed.

The annual energy demands for space heating and cooling amount to 135.5 MW h/year and 75.7 MW h/year, respectively. During this period, there were eight units in operation and the total conditioned area was approximately 3000 m^2. The hourly profile of the CO_2 intensity of electricity was provided for Switzerland by Electricity Maps [21].

Three thermal networks supply/remove heat to/from NEST. During the heating season, a medium temperature grid supplies heat at

Fig. 2. The building demonstrator NEST. © Zooey Braun, Stuttgart.

35 – 38 °C to the radiant systems and to the Air Handling Units (AHUs). The same terminal units and the AHUs are supplied with cold water at 6 °C during the cooling season. A high-temperature grid supplies heat for domestic hot water production with supply temperature ranging between 55 and 60 °C all year long. For sake of simplicity, the heat demand for domestic hot water production was ignored in this study. A water-to-water heat pump (WWHP) can extract heat from the low-temperature grid and supply the heating system at medium temperature. The WWHP can also extract heat from a 69 m^3 ice storage using a water-glycol mixture in a separate circuit. The low-temperature grid can also exchange heat (extract in winter and reject in summer) with two borehole heat exchangers. In this study, the latter were not considered, and an air chiller was considered as the only alternative to the ice storage to provide space cooling. This choice was made to obtain general results that do not depend completely on the case study. The cooling capacity of the air chiller was not set a priori, i.e., it was an output of the optimization.

Fig. 4 shows the ice storage connected to the low-temperature grid of NEST: on the left there is a photo taken during construction works, and on the right there is a photo of the coils inside the storage.

Table 1
Dimensions of the selected set of ice storage systems.

V (m^3)	D (m)	h (m)	S (m^2)	S_l (m^2)	S_{tot} (m^2)	S/V (m^{-1})
70	5.63	2.81	24.9	49.8	99.5	1.42
140	7.09	3.55	39.5	79.0	158.0	1.13
210	8.12	4.06	51.7	103.5	207.0	0.99
280	8.93	4.47	62.7	125.4	250.7	0.90
350	9.62	4.81	72.7	145.5	291.0	0.83
420	10.23	5.11	82.1	164.3	328.6	0.78
490	10.77	5.38	91.0	182.1	364.1	0.74

3.2. Parameters

The value of the electricity price was assumed to be $\lambda_{imp} = 0.238$ CHF/kW h, which is the average price in the municipality of Dübendorf (Switzerland) for commercial customers of type C3 (medium-sized enterprises with maximum energy consumption 150'000 kW h/year and maximum peak power of 50 kW according to the open data provided by the Federal Electricity Commission of Switzerland [22]). The investment cost for the ice storage includes excavation costs, the concrete casing and the heat exchangers. Two cost functions were considered: one proposed by Allan et al. [8] and one taken from the technical report of the BigIce project [23]. The lifetime of the storage was assumed to be equal to 50 years [24]. The additional costs for insulating the ice storage were not considered. Seven sizes were chosen, all multiples of the size of the system installed at Empa - as described in the previous section. To have comparable systems, it was assumed to keep the cylindrical shape and the same ratio between height and diameter, equal to 0.5. Table 1 shows the main geometric quantities that characterize the selected systems. As the last column of the Table shows, higher volumes have significantly lower S/V ratios. Thus, it is expected that heat gains will affect small-sized systems more than big ones.

The specific investment cost of the air chiller was assumed to be equal to 576 CHF/kW with a lifetime of 20 years, which is a common assumption for heat pumps and chillers (e.g. [11]). The performance of the glycol-to-water heat pump which extracts heat from the ice storage was derived from measured data of the low-temperature heat pump installed at NEST. The coefficients c_0 and c_1 of the correlation shown in Eq. (12) were obtained using a linear regression from one-year data (01/01/2021 – 31/12/2021) resampled at a 15-minute resolution, as shown in Fig. 5.

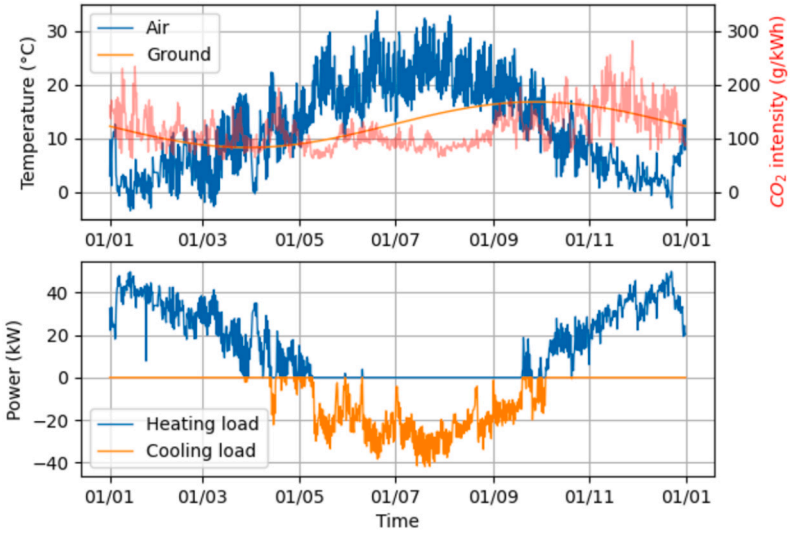

Fig. 3. Boundary conditions: outdoor air temperature, ground temperature 3 m below surface, CO_2 intensity of electricity, heating and cooling loads. (For interpretation of the colors in the figure(s), the reader is referred to the web version of this article.)

Fig. 4. The ice storage connected to the NEST energy system: construction works (left) and coils inside the storage (right).

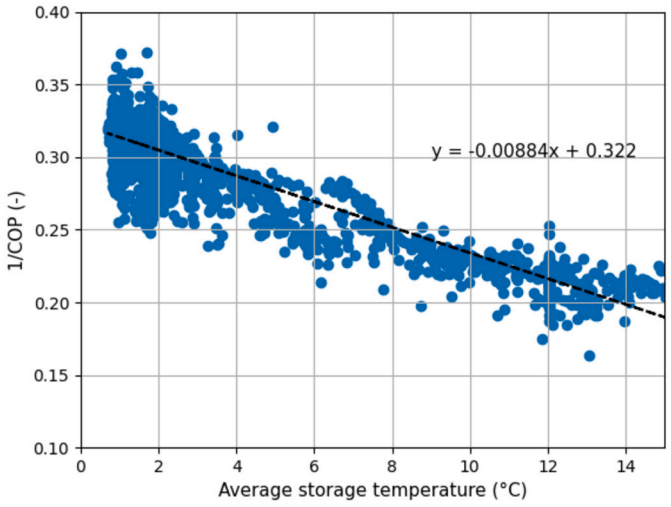

Fig. 5. Regression from measured data of the glycol-to-water heat pump in NEST.

To facilitate the interpretation of results, the same law has been used for the air-source heat pump. In this case, the heat source corresponds to the outdoor air instead of the average temperature in the storage. The performance of the air chiller was taken from Joe and Karava [25].

A high value of M in Equation (1) was found to be crucial to avoid numerical issues leading to physically inconsistent solutions where ice was completely melting in one time step. After a sensitivity analysis, this value was set to 10^4. Two heat transfer coefficients U have been considered for the energy balance constraints, i.e., Equations (2) and (3). All results shown in the manuscript refer to a thermally insulated storage, where $U = 0.5$ W/(m^2 K). Section 4.1.3 compares these results with those obtained by a storage with no thermal insulation. Such a condition is represented by a heat transfer coefficient of $U = 2.0$ W/(m^2 K), due to the thermal resistance offered by the ground around the storage. This value was also used in the model validation in Appendix A. In Equation (4) we set $\Delta T_{disch} = 10$ K and $\Delta T_{ch} = 5$ K based on monitored peak heat flow rates exchanged by the ice storage installed at Empa. The maximum heat transfer rate $U_{hx}A_{hx}$ has been assumed to increase linearly with the volume of the storage. For these systems, a linearly decreasing relationship of the U_{hx} coefficient as the ice level increases might be more suitable [26]. Although the influence of ice level on the maximum heat transfer rate in the storage might change the optimal operation strategies of the storage, this simplification was due to the case study and seems to be reasonable for two reasons. First, the higher thermal resistivity of the ice layer when ice grows is partially compensated by the higher contact area on the outside of the tube [27]. Second, in all scenarios, the ice approaches its maximum level at the end of the winter, when heat loads are low.

4. Results and discussion

This section is divided into three parts. The first one discusses the effects of storage size, CO_2 intensity of electricity and thermal storage insulation on the optimal operation of the system. The second section deals with the choice of the cost-optimal storage size. In the third section, a broader discussion focuses on the impact of our assumptions on the validity of the results.

4.1. Optimal operation

Figs. 6–8 describe the optimal operation of the energy system, each using three subplots. The first one shows the evolution over time of the ice level and average temperature in the storage. The second and third subplots show the contributions of the Air-Source Heat Pump (ASHP) and the WWHP to the heating supply, as well as those of the air chiller and the free cooling provided by the ice storage to meet the cooling supply.

4.1.1. Effect of storage size

Fig. 6 shows the optimal operation of the ice storage considering two sizes: 140 m^3 (twice the volume of the storage installed at Empa) and 420 m^3, i.e., three times bigger. Fig. 6(a) shows the annual pattern of ice level (black lines) and of the average temperature (red lines) in the storage, with the dashed lines representing the smaller storage.

It can be seen that the strategy to form ice, i.e., charging the cold storage, is similar for both sizes: the water is frozen, increasing the level of ice in the storage, during the second part of the heating season, in order to provide free cooling during early summer. When the ice is completely melted, the water is warmed up to exploit residual cooling energy available via sensible heat exchange. The main advantage of this strategy is that the frozen storage can be then used in the first part of the cooling season to provide “free cooling”, thereby saving electricity that would otherwise be needed to operate the air-cooled chiller. According to Equations (7) and (8), heat can be rejected into the storage until the temperature reaches $T_{cool,su}$, i.e., 6 °C in this case. Above this temperature, the ice storage can be only used as a heat source for the WWHP. However, during winter there is no cooling demand and higher water temperature makes the storage a preferable heat source compared to the air, as it leads to a higher heating COP. A higher water temperature also means lower heat gains from the ground, thereby increasing the

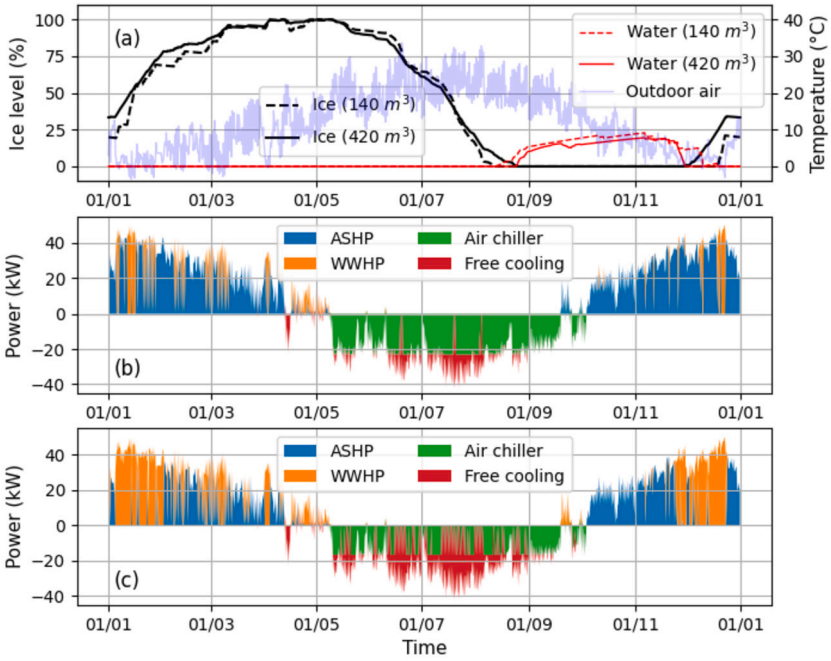

Fig. 6. Optimal operation of ice storage systems of different size: (a) ice level and water temperature patterns; (b) heat flow profiles with a storage volume of 140 m^3 and (c) heat flow profiles with a storage volume of 420 m^3.

storage efficiency. However, excessive use of the WWHP instead of the ASHP would in turn decrease the temperature in the storage, thus reducing the electricity savings in the subsequent period. Therefore, there is a trade-off between ASHP and WWHP use during the heating season. The optimal solution consists in letting the ground warm up the water and concentrate the icing periods during the coldest days, when the outdoor air temperature is below 0 °C and ice becomes a warmer heat source. This behavior can be observed in Fig. 6(b), where the WWHP operation (orange area) corresponds to the periods with lowest air temperature - see profile in 6(a). The bigger the storage, the longer the time needed for freezing all the water in the storage, and the higher the WWHP use in the overall heat supply. This can clearly be observed by comparing the orange area in Fig. 6(b) and 6(c). For the same reason, freezing starts slightly earlier when the 420 m^3 storage is used, i.e., at the end of November instead of mid December. A few days before the freezing process starts, the water reaches its maximum value, which is 9.2 °C with the smallest storage, and 8.0 °C with the largest one. Results show a decreasing trend of the maximum temperature with increasing volume. The larger the amount of ice accumulated in the storage, the higher the FCR (cooling provided by the ice storage out of the overall cooling demand): only 17.2% for the 140 m^3 storage, and 48.5% when its volume is 420 m^3. The seasonal efficiency increases as well from 73.9% to 77.7%, due to the lower S/V ratio. The higher FCR can be recognized clearly by comparing the red area to the overall cooling demand (red and green) in Figs. 6(b) and 6(c). In both cases (small and big storage), the ice storage is employed to cover the peak cooling demand, thus allowing a reduction in the cooling capacity of the air chiller and its related capital costs. More details on the optimal design will be provided in Section 4.2. For the case study considered, the optimal solution is not constrained by Equation (5). In fact, even when the smallest ice storage is employed (70 m^3), the cooling peak load (approximately 40 kW) is lower than the maximum heat transfer rate during the discharging phase (61.6 kW).

4.1.2. *Effect of* CO_2 *price*

Fig. 7 shows that increasing the cost of CO_2 emissions does not significantly affect the optimal operation of the ice storage. In fact, the pattern of the ice level shown in Fig. 7(a) is almost the same for a simulation without a CO_2 emissions price, and one with a relatively high price (250 CHF/t). However, two differences can be observed in the second part of the year, when ice in the storage has melted completely and water is used either to provide space cooling or as a heat source for the WWHP. When the CO_2 emissions cost of 250 CHF/t is employed, the optimization drives the storage towards higher temperatures (continuous red line in Fig. 7(a)) and the use of the WWHP (orange area in Fig. 7(c)) increases compared to the case when CO_2 can be emitted for free (Fig. 7(b)). In the latter case, the economic optimum consists in using the water as a heat source when heating is needed during late September, so that during the following week the water in the storage is cold enough to provide free cooling. With this strategy, the maximum water temperature reached by the storage is 9.2 °C. Conversely, with a CO_2 price of 250 CHF/t, the first heating loads are supplied by the air source heat pump and the water in the storage is heated by the ground up to 10.8 °C. The peak temperature is reached during the last week of November (continuous red line in Fig. 7(a)). Then, water is used as a source for the heat pump (orange area in Fig. 7(c)). This result is also due to the higher CO_2 intensity of electricity during the winter months. With these boundary conditions, it is preferable to have a higher COP during heating operations instead of providing free-cooling during late summer. It is worth noting that the CO_2 savings obtained through such operational changes are rather small (only 14 kg/year) if compared to the overall CO_2 emissions associated with space heating and cooling of the considered building (7419 kg/y in the baseline case without ice storage).

4.1.3. *Effect of thermal insulation*

All the results presented so far refer to a thermally insulated storage with $U = 0.5$ W/(m^2 K). Here we compare this case to the storage with negligible thermal insulation, i.e., with $U = 2.0$ W/(m^2 K). This value roughly corresponds to the one of the real system installed in the Empa Campus. Fig. 8 compares the two levels of thermal insulation and shows how they affect the optimal control policy of the 210 m^3 ice storage.

The optimal operation differs significantly when the storage is less thermally insulated. The slope of the continuous red line in Fig. 8(a) shows that when the ice is completely melted, the ground heats the water more rapidly. Although this might appear as a disadvantage because the ice storage cannot be used as effectively for free cooling, the storage is used as a ground-coupled water tank during the first part of the heat-

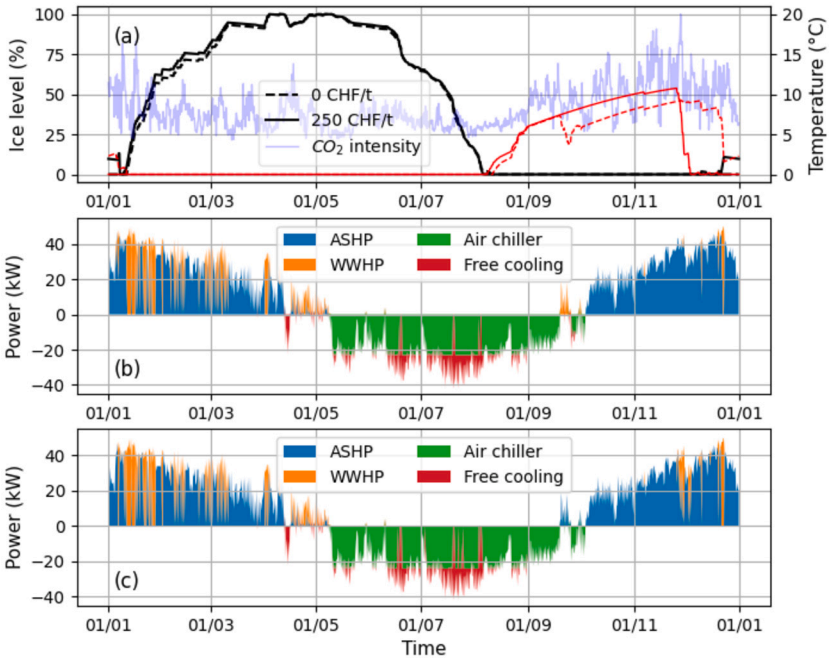

Fig. 7. Optimal operation of a 140 m^3 ice storage with different CO_2 prices: (a) ice level and water temperature patterns; (b) heat flow profiles with 0 CHF/t and (c) heat flow profiles with 250 CHF/t.

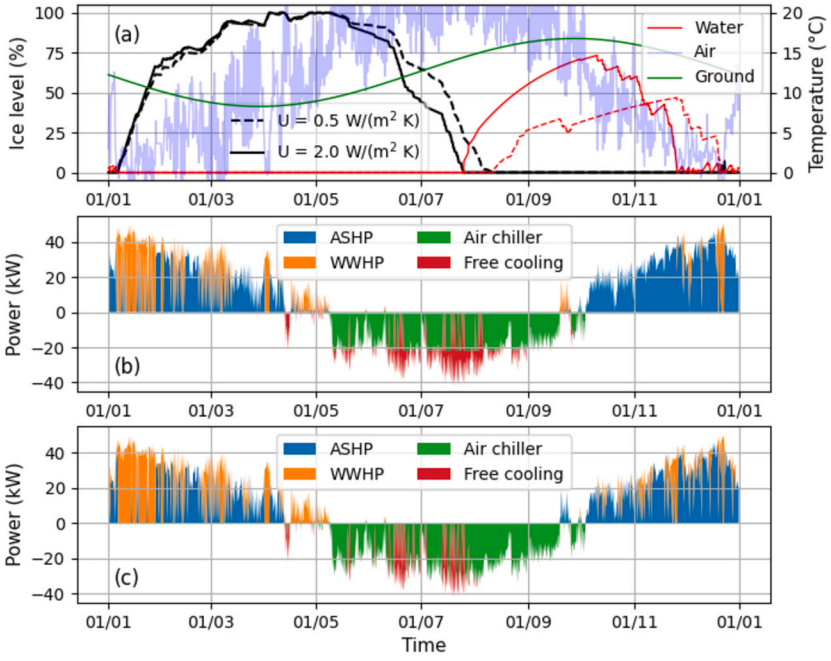

Fig. 8. Optimal operation of a 210 m^3 ice storage with different thermal insulation: (a) ice level and water temperature patterns; (b) heat flow profiles with high thermal insulation and (c) heat flow profiles with negligible thermal insulation.

ing season (October and November), which does not occur for systems with a higher thermal insulation. Moreover, due to the high temperature reached by the water just before the start of the heating season (almost 15 °C), the WWHP can access an often more convenient source than the ASHP. This behavior is favored by the ground temperature profile (green line), which reaches its peak exactly in the same period of the year. Compared to the case with thermal insulation, the ice in the storage melts faster, due to the higher heat gains from the surrounding ground. Consequently, the seasonal efficiency of the storage η_{st} drops from 71.4% to 37.4% and FCR decreases from 24.8% to 18.0%. Similar reductions occur for systems of different size. Table 2 shows the same key performance indicators for all storage volumes considered and for both thermal insulation levels of the storage. It can be observed that the trends are similar, and that the biggest storage fulfills only 43.8% of the cooling demand when the storage is not thermally insulated, compared to 56.5% of the reference case with thermal insulation. To achieve this cost-optimal FCR, much more heat must be removed by the storage with the WWHP. In fact, due to the lower insulation level, the seasonal efficiency drops from 78.4% to 45.6%. This leads to using the WWHP for longer periods, as more heat must be removed from the storage. As a result, the ASHP operation is concentrated during periods with higher air temperature, thus achieving a higher Seasonal Coefficient Of Perfor-

Table 2
Energy-related annual performance indicators of the ice storage with and without thermal insulation.

	U = 0.5 W/(m² K)				U = 2.0 W/(m² K)			
V m³	SCOP -	SEER -	FCR %	η_{st} %	SCOP -	SEER -	FCR %	η_{st} %
0	3.54	2.99	0.0%	-	3.54	2.99	0.0%	-
70	3.59	3.02	9.6%	55.0%	3.61	3.02	6.1%	29.5%
140	3.63	3.07	17.2%	71.5%	3.66	3.08	12.1%	33.7%
210	3.69	3.15	24.8%	71.4%	3.73	3.13	18.0%	37.4%
280	3.75	3.19	32.7%	75.7%	3.77	3.18	24.5%	42.6%
350	3.81	3.28	40.6%	76.8%	3.90	3.25	30.5%	43.0%
420	3.88	3.34	48.4%	77.7%	4.10	3.30	37.0%	44.0%
490	3.97	3.45	56.5%	78.4%	4.24	3.33	43.8%	45.6%

Table 3
Costs and CO_2 emissions of ice storage systems of different sizes with and without thermal insulation.

U = 0.5 W/(m² K)						
V m³	P_{chill} kW	OPEX kCHF/y	CAPEX kCHF/y	LCOE CHF/MWh	E_{CO_2} kg/y	ΔE_{CO_2} %
0	41.9	15.9	1.2	80.9	7419	
70	26.7	15.2	2.9	85.7	7165	-3.4%
140	23.2	14.7	3.5	86.1	6964	-6.1%
210	21.9	14.1	3.9	85.4	6764	-8.8%
280	19.2	13.6	4.1	84.1	6589	-11.2%
350	18.8	13.1	4.4	82.8	6418	-13.5%
420	16.8	12.7	4.5	81.5	6266	-15.5%
490	16.8	12.3	4.7	80.1	6120	-17.5%
U = 2.0 W/(m² K)						
V m³	P_{chill} kW	OPEX kCHF/y	CAPEX kCHF/y	LCOE CHF/MWh	E_{CO_2} kg/y	ΔE_{CO_2} %
0	41.9	15.9	1.2	80.9	7419	
70	33.8	15.4	3.1	87.7	7235	-2.5%
140	33.8	15.0	3.8	89.3	7074	-4.7%
210	33.8	14.6	4.2	89.2	6922	-6.7%
280	33.8	14.2	4.5	88.6	6755	-8.9%
350	33.8	13.8	4.8	88.0	6644	-10.4%
420	33.8	13.5	5.0	87.4	6559	-11.6%
490	33.8	13.2	5.1	87.0	6487	-12.6%

mance (SCOP) compared to the thermally insulated case. Table 2 shows that SCOP of the ASHP goes from 3.59 to 3.97 when $U = 0.5$ W/(m² K), and the range increases to 3.61 up to 4.24 when $U = 2.0$ W/(m² K). The difference increases with increasing volume, thus partially compensating for the higher amount of electricity needed to operate storage due to lower thermal insulation. A similar observation holds true for Seasonal Energy Efficieny Ratio (SEER) of the air chiller, although during cooling operations the difference between ice systems with and without thermal insulation is less pronounced.

4.2. Optimal size

Fig. 9 shows the effect of the storage size and of the cost function adopted for the ice storage on the LCOE. The latter accounts for both capital and operational cost for space heating and cooling and both with and without thermal insulation. Colored, continuous lines indicate LCOE of the system assuming a CO_2 emission price of 125 CHF/t. As shown in Fig. 7, changing this price does not affect the optimal operation strategy significantly. Therefore, increasing (decreasing) this price would only shift the LCOE curve upwards (downwards). The black dashed line indicates CO_2 emissions savings compared to a reference scenario without ice storage.

As far as the LCOE is concerned, the trend is highly dependent on the cost function used for the ice storage investment. The blue lines refer to an LCOE calculated using the logarithmic curve proposed by Allan et al. [8] for the investment cost, whereas the orange lines are calculated considering a linear cost function as proposed by Carbonell et al. [23]. In the first case, the LCOE increases until it reaches a peak and then decreases linearly with increasing volume. Such decrease is linked to the reduction in the capital cost for the air chiller and, most importantly, to the reduction in the Operational expenditure (OPEX), as shown in Table 3. This decrease of the LCOE with increasing size does not compensate the initial investment in case of uninsulated storage -9(a)-, whereas it does when the storage is insulated, when the biggest size is employed (490 m³) - see Fig. 9(b). When the linear relationship between cost and size of the ice is used, a completely different LCOE trend appears. In this case, the cost savings due to free cooling in summer do not compensate the Capital expenditure (CAPEX), thus leading to a monotonically increasing LCOE. The reduction in CO_2 emissions compared to the reference case without ice storage is approximately 12.5% without

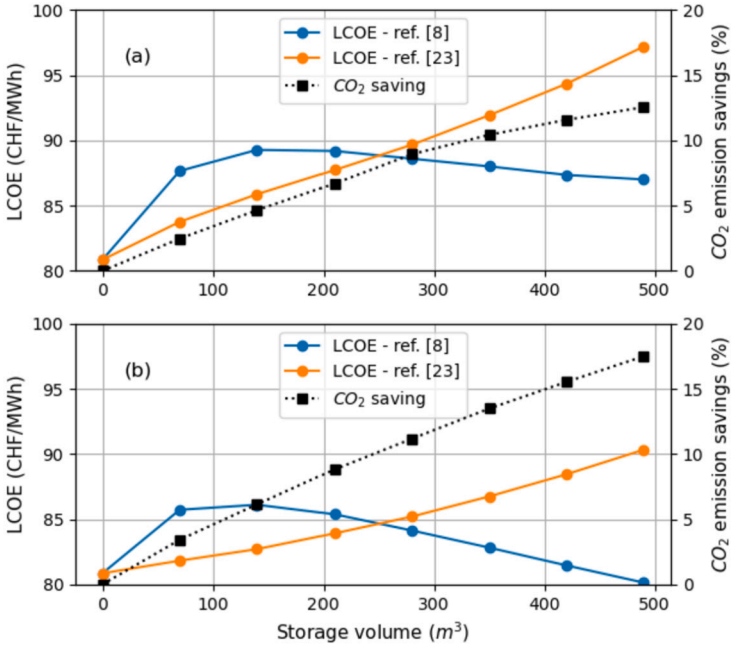

Fig. 9. Effect of storage size and cost function on LCOE and annual CO_2 emission savings (a) without and (b) with thermal insulation.

thermal insulation and reaches 17.5% when the concrete casing is thermally insulated. CO_2 emissions saved by smaller ice storage systems are shown in Table 3. While in these graph the CO_2 emission savings appear to have a linearly increasing trend in first part with smaller volumes, it can be noticed that the curve starts to bend with larger volumes, indicating as expected that there is an upper limit to the amount of CO_2 emissions an ice storage can actually save, which depends mostly on the cooling demand and ice storage construction properties.

4.3. Remarks

The results shown in this paper rely on the assumption that the heat transfer coefficient of the heat exchanger inside the ice storage is constant. This assumption was made not only because the Empa's monitored system does not show a significant correlation between the ice level and thermal resistance - as discussed in Section 2.1.1, but also because this would require a higher computational effort. Furthermore, there are only a few available correlations in the literature, and they mostly refer to ice storages with different types of heat exchangers [26].

In general, results showed that a good operation strategy consists in using a heat pump to form ice at the end of the winter to avoid using the air chiller in the first part of the cooling season. However, results also showed that the ice storage can be operated differently depending on its volume, on CO_2 price and on the level of thermal insulation. Larger storage volumes lead the cost-optimal operation to start the ice-forming process earlier in the winter. The length of the icing period depends on the trade-off between reducing heat gains from the ground (i.e., increasing storage efficiency) and reducing the heat pump's electricity expenditure. In fact, storing ice for too long might result in unnecessary waste of energy, but it could also be a more efficient alternative to using the air as a source when the air temperature is below 0 °C.

The optimization was formulated with 8-hourly time-step, as this was found to be the best trade-off between computational effort and accuracy of the results. This means periodical fluctuations were captured at different scales, at most with daily resolution. The prominent periodical use of the storage was at seasonal scale, although some shorter term use of the storage (weekly) appeared, obviously with a partial charge and discharge of the storage. For instance, it can be seen in Figs. 6, 7 and 8 that in April and late September the storage was discharged to supply cold water during warmer Spring or Autumn days.

Results showed that CO_2 emissions price does not lead to a further significant reduction in emissions in the considered scenario, probably due to the seasonal fluctuation in CO_2 intensity of electricity, higher in winter than in summer. Therefore, shifting loads from the cooling to the heating season have a limited contribution in the CO_2 emissions reduction aspect. Considering the evolution of energy systems, where an increased penetration of solar electricity generation that could increase this seasonal difference is expected, ice storage might play a different role. While the seasonal benefits might be reduced, its use as a daily energy storage might become even more attractive.

The previous Section has shown that the optimal size is highly dependent on the ice storage investment cost function used to calculate the LCOE. Costs may vary depending on the case study, and space constraints might set an upper bound to the possible storage size. The operational cost reduction depends mainly on the amount of free cooling supplied by the storage with respect to the cooling demand. In the case considered, the ratio between heating and cooling loads was approximately equal to 1.8. The effect of climate on the energy demand for space heating and cooling seems to be therefore an important aspect to investigate. Cooling-dominated buildings located in climates with very cold winters and very hot summers could be the most promising candidates for an economically sustainable application of long-term ice storage. Other aspects, such as efficiency improvements during the heating season (increased COPs during cold winter days) reduce operating costs further, and can be put in place through appropriate control strategies that consider long-term system performance.

5. Conclusions

This paper presented an optimization process for determining the best sizing and operation of seasonal ice storage systems. The proposed framework, based on the formulation of a quadratically-constrained mixed integer programming problem describing the energy system's physical behavior, explicitly models the latent and sensible phases of the ice storage, computing the storage temperature and liquid fraction to determine the efficiency of the storage and of the connected heat pump. Despite the increased complexity compared to other state-of-the-art methods, the proposed formulation could converge to a solution within a reasonable time, in the order of two hours. Concerning the optimal operation, results showed that:

- Regardless of the considered storage size, the ice storage is used to supply free cooling in early summer by melting the ice formed during the heating season;
- It is generally best to form the ice during late winter and when the air temperature drops below 0 °C, as this would result in the maximum state of charge at the beginning of the cooling season with the least amount of heat gains reducing the efficiency of the storage, and having higher COP compared to an alternative air-source heat pumps.
- The ice storage can shave the seasonal cooling peak load, reducing the capacity of the installed air chiller.

Concerning the optimal design of the storage, two different empirical cost functions were considered in this study. In this regard, results showed that:

- Due to the seasonal nature of the storage, and therefore the limited amount of charging/discharging cycles over the storage's lifetime, the reduction in operating costs due to free cooling hardly compensates for the investment costs, at least under current electricity prices and storage costs. When a logarithmic cost function was employed, the best size corresponds to the largest volume, due to the economies of scale. When a linear cost function was employed, the lowest LCOE was achieved without ice storage, indicating that it is not a cost-effective technology on a seasonal scale.
- For the case study considered, the largest storage yielded an annual electricity demand reduction of 23.0% for space heating and cooling combined, and a free cooling ratio of 56.5%. The corresponding CO_2 emissions saved were limited to 17.5% due to the seasonal variation in CO_2 intensity of the electricity in Switzerland, being lower in summer compared to winter.
- When the ice storage tank is not insulated, its seasonal efficiency is drastically reduced, but the year-round operating costs do not decrease as much. This is because this optimization employs a different operation strategy that partially offsets the higher storage heat gains and loss of efficiency in providing cooling, by increasing the temperature of the water in winter and therefore improving the heat pump performance in the heating season.

Future work will focus on comparing the results achieved for the ice storage solutions with other seasonal thermal energy storage alternatives, such as water tanks, borehole fields, and other latent materials.

CRediT authorship contribution statement

Jacopo Vivian: Conceptualization, Data curation, Methodology, Software, Visualization, Writing – original draft, Writing – review & editing. **Philipp Heer:** Resources, Supervision, Writing – review & editing. **Massimo Fiorentini:** Conceptualization, Funding acquisition, Methodology, Resources, Supervision, Writing – review & editing.

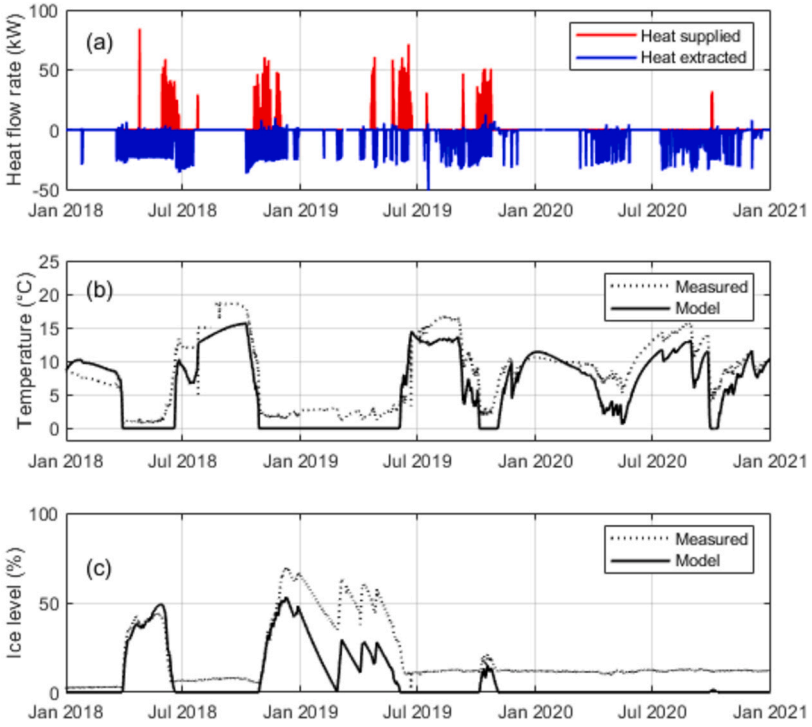

Fig. A.1. Comparison between model output and measured data during three years of operation (1 Jan 2018 - 31 Dec 2020) of NEST ice storage: (a) heat extracted from /supplied to the ice storage; (b) average temperature in the storage; (c) level of water surface.

Declaration of competing interest

The authors declare that they have no known competing financial interests or personal relationships that could have appeared to influence the work reported in this paper.

Acknowledgements

The authors would like to acknowledge the financial support of the Swiss National Science Foundation (SNSF), through the Sinergia project no. CRSII5_202239 and of the Swiss Federal Office of Energy SFOE grant Nr. SI/502259-01.

Appendix A. Validation of the simplified ice storage model

Fig. A.1 compares the simulation output of the simplified model described in Section 3 with measurements taken from the ice storage installed in NEST (see Section 3 for more details) during three years of operation, between 01/01/2018 and 31/12/2020. Fig. A.1(a) shows the heat rejected into the storage (red) during the cooling season and the heat extracted by the heat pump (blue) during the heating season, which are both inputs to the model. Fig. A.1(b) shows the thermal response in terms of average temperature of the ice storage model (continuous line) against the measured one (dotted line). The $RMSE$ between the temperature profiles over three years is 4.7 K, whereas the R^2 is 0.55.

The ice storage is also equipped with a radar sensor for level measurement, installed on top of the storage. The latter measures the distance d of the water surface from the sensor itself, which changes over time due to the changing ice fraction in the storage. Since the density of ice ($\rho_i = 920$ kg/m^3) is significantly lower than that of water ($\rho_w = 1000$ kg/m^3), the water surface level increases with growing ice fraction. Therefore, the sensor distance d decreases as long as the water freezes. The equivalent density in the storage can be expressed as:

$$\rho(t) = \rho_w \epsilon(t) + \rho_i (1 - \epsilon(t)) \tag{A.1}$$

While the volume of water changes over time depending on the ice fraction, the mass of water in the storage is conserved.

$$\rho_w V_{st} = \rho(t) A (h - d(t)) \tag{A.2}$$

where h is the height of the storage and V_{st} is the nominal volume of the storage - in this case 69 m^3.

Replacing the equivalent density ρ in Eq. (A.2) allows to estimate the water fraction (thus also the ice fraction) in the storage using the distance between water surface and level sensor:

$$\epsilon(t) = \frac{\frac{\rho_w V}{A(h-d(t))} - \rho_i}{\rho_w - \rho_i} \tag{A.3}$$

Fig. A.1(c) compares the ice fraction $(1-\epsilon)$ calculated with Eq. (A.3) (dotted line) with that obtained using the ice storage model (continuous line). The comparison shows that the model is also able to predict the amount of ice present in the storage.

It is worth noting that some of the mismatches between the model and the experimental data is due to uncertainty in the measurements. For example, when the temperature of the storage is above 0 °C (e.g. Jan-2020 to Jul-2020), the measurement reports some ice in the storage, which is likely not present. Furthermore, both the average temperature and the water level profiles could be improved by performing a calibration test to get a better fit of the parameters of the model.

References

[1] L.F. Cabeza, I. Martorell, L. Miró, A.I. Fernández, C. Barreneche, L.F. Cabeza, A.I. Fernández, C. Barreneche, Introduction to thermal energy storage systems, in: Advances in Thermal Energy Storage Systems, Elsevier, 2021, pp. 1–33.

[2] T. Yang, W. Liu, G.J. Kramer, Q. Sun, Seasonal thermal energy storage: a techno-economic literature review, Renew. Sustain. Energy Rev. 139 (2021) 110732, https://doi.org/10.1016/j.rser.2021.110732.

[3] D. Carbonell, D. Philippen, M. Haller, S. Brunold, Modeling of an ice storage buried in the ground for solar heating applications. Validations with one year of monitored data from a pilot plant, Sol. Energy 125 (2016) 398–414, https://doi.org/10.1016/j.solener.2015.12.009.

[4] Z. Nie, W. Cheng, G. Zhou, X. Chen, C.B. Yan, F. Gao, Consistency guaranteed two-timescale decision and optimization of HVAC system with ice storage, Int. J. Electr.

Power Energy Syst. 141 (2022) 108115, https://doi.org/10.1016/J.IJEPES.2022.108115.
[5] P. D'Agaro, M. Libralato, G. Toffoletti, G. Cortella, Ice thermal energy storage for electricity peak shaving in a commercial refrigeration/HVAC unit, International Institute of Refrigeration (IIR), Vicenza (IT), 2021, https://doi.org/10.18462/IIR.TPTPR.2021.2038.
[6] D. Erdemir, N. Altuntop, Y.A. Çengel, Experimental investigation on the effect of ice storage system on electricity consumption cost for a hypermarket, Energy Build. 251 (2021) 111368, https://doi.org/10.1016/J.ENBUILD.2021.111368.
[7] M. Griesbach, A. König-Haagen, D. Brüggemann, Numerical analysis of a combined heat pump ice energy storage system without solar benefit – analytical validation and comparison with long term experimental data over one year, Appl. Therm. Eng. 213 (2022) 118696, https://doi.org/10.1016/J.APPLTHERMALENG.2022.118696.
[8] J. Allan, L. Croce, R. Dott, G. Georges, P. Heer, Calculating the heat loss coefficients for performance modelling of seasonal ice thermal storage, J. Energy Storage 52 (2022) 104528, https://doi.org/10.1016/j.est.2022.104528.
[9] C. Yan, W. Shi, X. Li, Y. Zhao, Optimal design and application of a compound cold storage system combining seasonal ice storage and chilled water storage, Appl. Energy 171 (2016) 1–11, https://doi.org/10.1016/J.APENERGY.2016.03.005.
[10] P. Gabrielli, M. Gazzani, E. Martelli, M. Mazzotti, Optimal design of multi-energy systems with seasonal storage, Appl. Energy 219 (2018) 408–424, https://doi.org/10.1016/J.APENERGY.2017.07.142.
[11] M. Fiorentini, P. Heer, L. Baldini, Design optimization of a district heating and cooling system with a borehole seasonal thermal energy storage, Energy 262 (2023) 125464, https://doi.org/10.1016/j.energy.2022.125464.
[12] M. Fiorentini, J. Vivian, P. Heer, L. Baldini, Design and optimal integration of seasonal borehole thermal energy storage in district heating and cooling networks, in: CLIMA 2022 The 14th REHVA HVAC World Congress, 2022.
[13] K. Heine, P.C. Tabares-Velasco, M. Deru, Design and dispatch optimization of packaged ice storage systems within a connected community, Appl. Energy 298 (2021) 117147, https://doi.org/10.1016/j.apenergy.2021.117147.
[14] S. Mazzoni, J.Y. Sze, B. Nastasi, S. Ooi, U. Desideri, A. Romagnoli, A techno-economic assessment on the adoption of latent heat thermal energy storage systems for district cooling optimal dispatch 'i&' operations, Appl. Energy 289 (2021) 116646, https://doi.org/10.1016/j.apenergy.2021.116646.
[15] A. Beghi, L. Cecchinato, M. Rampazzo, F. Simmini, Energy efficient control of HVAC systems with ice cold thermal energy storage, J. Process Control 24 (6) (2014) 773–781, https://doi.org/10.1016/j.jprocont.2014.01.008.
[16] M. Fiorentini, P. Cooper, Z. Ma, Development and optimization of an innovative HVAC system with integrated PVT and PCM thermal storage for a net-zero energy retrofitted house, Energy Build. 94 (2015) 21–32, https://doi.org/10.1016/j.enbuild.2015.02.018.
[17] X. Fang, K. Huang, G. Feng, W. Cai, J. Song, H. Li, G. Li, Experimental and numerical research on the performance of a seasonal ice storage device in summer residential rooms of northeast China, Sustain. Cities Soc. 75 (2021) 103334, https://doi.org/10.1016/j.scs.2021.103334.
[18] N. Bianco, A. Fragnito, M. Iasiello, G.M. Mauro, L. Mongibello, Multi-objective optimization of a phase change material-based shell-and-tube heat exchanger for cold thermal energy storage: experiments and numerical modeling, Appl. Therm. Eng. 215 (2022) 119047, https://doi.org/10.1016/j.applthermaleng.2022.119047, https://linkinghub.elsevier.com/retrieve/pii/S1359431122009796.
[19] A. Saito, Recent advances in research on cold thermal energy storage, Int. J. Refrig. 25 (2) (2002) 177–189, https://doi.org/10.1016/S0140-7007(01)00078-0.
[20] Gurobi Optimization, LLC, Gurobi Optimizer Reference Manual, https://www.gurobi.com, 2022.
[21] Electricity maps, https://www.electricitymaps.com. (Accessed 14 December 2022).
[22] Switzerland's electricity tariffs, https://www.strompreis.elcom.admin.ch. (Accessed 1 December 2022).
[23] D. Carbonell, M. Schubert, M. Neugebauer, BigIce - assessment of solar-ice systems for multi-family and tertiary buildings, Tech. Rep. SFOE SI/501726-01, 2021, https://www.aramis.admin.ch/Default?DocumentID=67998I&Load=true.
[24] M. Berger, B. Schroeteler, H. Sperle, P. Püntener, T. Felder, J. Worlitschek, Assessment of residential scale renewable heating solutions with thermal energy storages, Energy 244 (2022) 122618, https://doi.org/10.1016/j.energy.2021.122618.
[25] J. Joe, P. Karava, A model predictive control strategy to optimize the performance of radiant floor heating and cooling systems in office buildings, Appl. Energy 245 (2019) 65–77, https://doi.org/10.1016/j.apenergy.2019.03.209.
[26] D. Carbonell, M. Granzotto, M.D. Philippen, M.Y. Haller, M. Battaglia, Experimental and numerical investigations of heat exchangers in ice storages for combined solar and heat pump systems, in: Proceedings of EuroSun2016, International Solar Energy Society, Palma de Mallorca, Spain, 2016, pp. 1–12, http://proceedings.ises.org/citation?doi=eurosun.2016.03.01.
[27] D. Carbonell, D. Philippen, E. Frank, M. Granzotto, M. Haller, Simulation of combined solar thermal, heat pump, ice storage and waste water heat recovery systems. Design criteria and parametric studies, in: Proceedings of the EuroSun 2014 Conference, International Solar Energy Society, Aix-les-Bains, France, 2015, pp. 1–10, http://proceedings.ises.org/citation?doi=eurosun.2014.03.04.